Photocatalytic hydrogen production from water-methanol and glycerol mixtures using $Pd/TiO_2(-WO_3)$ catalysts and validation in a solar pilot plant

S.Y.Toledo-Camacho[a], A.Rey[b], M.I.Maldonado[c], J.Llorca[d], S.Contreras[a], F.Medina[a]

[a] Departament d' Enginyeria Química, Universitat Rovira i Virgili, Av. Països Catalans, 26, Tarragona, 43007, Spain

[b] Departamento de Ingeniería Química y Química Física, Universidad de Extremadura, Av. Elvas s/n, 06006, Badajoz, Spain

[c] Plataforma Solar de Almería-CIEMAT, Carretera de Senés, km 4, 04200, Tabernas, Almería, Spain

[d] Institut de Tècniques Energètiques, Barcelona Research Center in Multiscale Science and Engineering, and Department of Chemical Engineering, Universitat Politécnica de Catalunya, 08019, Barcelona, Spain

Abstract

This paper is focused on the photocatalytic hydrogen production on $Pd/TiO_2(-WO_3)$ catalysts from water-methanol and water-glycerol mixtures under UVA and solar irradiation. The photodeposition method for Pd was studied varying conditions such as Pd amount, catalyst concentration and methanol concentration. The catalysts were tested at lab scale under simulated solar light and UVA radiation and also at large scale (25 L) under solar energy using a pilot-scale solar Compound Parabolic Collector (CPC). The catalysts characterization was performed by means of ICP-OES, N_2 adsorption–desorption isotherms, XRD, HR-TEM, XPS and DR–UV–Vis spectroscopy. Hydrogen evolution was monitored by on-line gas chromatography.From results it was found the Pd photodeposition method plays a key role to increase the hydrogen evolution, affecting parameters like the Pd amount deposited, the Pd nanoparticles size and dispersion. The highest quantum efficiency (ϕ) obtained in this study was 11.8% and 41.2% under simulated solar and UVA irradiation, respectively, using Pd(0.24 wt%)/P25 in an aqueous solution of methanol (50 vol%). In the pilot-scale solar CPC, for Pd(0.24 wt%)//P25 catalysts in 5 vol% of methanol or glycerol as sacrificial agents, the quantum yield were 2.1 and 2.2%, respectively. When the concentration of the sacrificial agents decreased to 0.37 vol%, the quantum yields were 1.3 and 2.4% for methanol and glycerol, respectively. Compared to literature, the low noble metal content of these catalysts (0.25 wt%) seems to be a competitive factor considering their high price.

Keywords: Photocatalysis, Hydrogen, Photodeposition, Sacrificial agents, Quantum efficiency

Introduction

The unlimited supply of solar energy presents us the challenge of developing materials and processes capable of absorbing and transforming this sort of energy into the new fuel for our modern wasteful energy lifestyle. Since Fujishima and Honda (1972) [1], photocatalytic hydrogen (H_2) production on semiconducting materials as titanium dioxide (TiO_2) has been not only a potential technology to achieve these challenges, but also an environmental friendly alternative to fossil fuels -H_2 combustion only produces water (H_2O)- [2,3].

On this regard, the interest toward H_2 settles on its high efficient energy conversion, its three times higher capacity of storing energy than natural gas and its easy conversion to other kind of energy [[3], [4], [5], [6]].

Although non-conventional methods for H_2 production are not mature enough, still expensive and present low efficiencies [4], currently prevails a motivation on investigating new technologies (or work on those that already exist) to make H_2 become the fuel of the future either near or without carbon dioxide (CO_2) emissions. Nowadays, although there is a vast scientific literature about photocatalytic H_2 production, efficiencies towards photocatalytic H_2 are still low. Therefore, it is necessary to continue the study of photocatalysts, either from the development of new materials or the modification of existing materials to improve both, the solar light absorption and the H_2 generation yield. Ever since Fujishima and Honda (1972), the investigative effort to improve this technology has transcended from the photocatalytic H_2 production by means of water splitting [1,5,6] up to organic compounds oxidation [[7], [8], [9], [10], [11], [12]], inorganic compounds [9], dyes [10,11], biomass [12,13] and also to real wastewater treatment [7,14].

Basically, the photocatalytic process occurring on the catalyst surface consists of three steps: (i) incident photons absorption: only if the photons incoming has an equal or higher energy than the band-gap (BG) of the catalyst, (ii) charges photoexcitation: photons photo-excite the electrons (e^-) located in the valence band (VB), which “jump” to the conduction band (CB), leaving in the VB positive holes (h^+), and (iii) charges migration: the e^-/h^+ pair migrate towards the catalyst surface where they could react in further reactions.

In water splitting, Kudo et al. [5] explained that in the Honda - Fujishima effect of water splitting on a TiO_2 electrode, the photogenerated e^- reduced H_2O molecules to produce H_2 on a Pt electrode. On the other hand, h^+ oxidized H_2O towards oxygen (O_2) on a TiO_2 electrode. Therefore, photocatalytic materials used for this purpose should have the bottom level of the CB more negative than the redox potential of H^+/H_2 (0 V vs. NHE) and the top level of the VB more positive than the redox potential of O_2/H_2O (1.23 V). Additionally, the BG of these materials should be not too wide and not too narrow in order to absorb light in the visible range and reduce recombination probabilities, respectively. Different photocatalysts meet these conditions such as ZrO_2, $KTaO_3$, $SrTiO_3$, TiO_2, ZnS, CdS, SiC [5]. However, some of them do not have the capacity to produce H_2 by water splitting or their efficiencies are still low, likely due to photo-corrosion or because some of the parameters mentioned above are not sufficient either absorbing visible light, avoiding recombination or producing H_2.

In this sense, different authors have explored the combination of two alternative ways to improve the efficiency towards H_2: (i) to use co-catalysts as noble metals (Pt, Au, Ag, Rh or Pd), transition metals, metal oxides or non-metal doping; and (ii) to use sacrificial agents like organic or inorganic compounds, biomass or municipal or industrial wastewater [[7], [8], [9],13,15]. It seems that this combination creates separately active

sites for photogenerated e^- and h^+. On one hand, the noble metal co-catalyst acts as an active site for the reaction between e^- and H cations (H^+) to produce H_2, and on the other hand, the h^+ act as an active site for the degradation of organic compounds.
In our previous paper [16], H_2 production from water-methanol mixtures was studied in a series of catalysts based on Pd/TiO_2-WO_3 under visible and UVA light, where Pd was added in very small amounts (around 0.01 wt%). In this paper, the photocatalytic H_2 production is also studied on a series of catalysts based on Pd/TiO_2-WO_3 using organic compounds as sacrificial agents. Firstly, the study focuses on the improvement of the Pd deposition, considering parameters such as Pd amount, catalyst concentration and methanol concentration during photodeposition. For comparison, H_2 production tests were done under solar simulated and UVA irradiation from water-methanol and water-glycerol mixtures. Secondly, the catalysts were tested at large scale with solar energy using a pilot-scale solar reactor from water-methanol and water-glycerol mixtures.

Experimental section

Materials

Supports of P25-WO_3 and titanate nanotubes (NT-WO_3) containing WO_3 were synthesized according to a previous work [17]. Titanium (IV) oxide, Aeroxide P25 (Acros Organics) (XRD analysis: 87.6% anatase and 12.4% rutile; 16.9–30 nm primary particle size) and Titanium dioxide, TiO_2-anatase (Pure anatase Probus) (XRD analysis: 88.3% anatase and 11.6% rutile; 53.4–85 nm primary particle size) were used for Pd/P25 and Pd/TiO_2-anatase, respectively. Palladium (II) chloride ($PdCl_2$, Johnson Matthey, metal purity 59.66%) was used as the starting material of palladium (Pd), which was diluted in hydrochloric acid (HCl) 37% (Analytical reagent from Fisher). For the catalyst based on Pd/WO_3, tungstic acid (H_2WO_4) (Aldrich, 99%) was used as the precursor of WO_3. Two kinds of water were used for water-methanol mixtures: tap water and milliQ water. Methanol was supplied by Sigma Aldrich (99.8% purity). With regard to H_2 generation test using real municipal wastewater, the water was directly taken after the secondary treatment of a municipal wastewater treatment plant (conductivity 2.37 mS/cm, total organic carbon (TOC): 109.2 mg/and pH 7.5).

Catalysts preparation

Pd was incorporated in the catalysts by photodeposition (PD) and by wetness impregnation (wi) -in some samples for comparative purposes-. The Pd PD was carried out in two different media: (1) water (PD-w) and (2) water-methanol (PD-m). For Pd PD-w, an aqueous solution of $PdCl_2$ in HCl was added to a glass flask and stirred for some minutes. Then, the corresponding catalytic support (P25-WO_3, NT-WO_3, TiO_2-anatase, P25 or WO_3) was added under continuous stirring. Afterward, the system, still under continuous stirring, was deaerated with argon (Ar) (50 ml/min) for 50 min and then irradiated with a UVA lamp (λ max~365 nm, 6 W) overnight (around 14 h). After irradiation, the solid particles were recovered by filtration, washed several times with distilled water and dried at room temperature. Pd PD-m was prepared following the procedure described above, using a water-methanol (1, 5 or 10 vol%) solution instead of pure water. The Pd wi was prepared as follows: 2 ml of milliQ plus a specific quantity of $PdCl_2$ containing the nominal amount of Pd (0.25 wt%) was stirred for 1 h. Afterward, 1 g of P25 was added to the solution above and stirred for 3 h. Later, this solution was placed in the oven at 80 °C for 12 h to remove the remaining water. The solid obtained was triturated, and the powder reduced in a vertical tube furnace (Hobersal TR-2B, power 2 kW, 220 V, 50/60 Hz. Temperature ramp: 25 °C, 2 °C/min, 300 °C (2 h); carrier gas: H_2 with flow rate of 30 ml/min).

Characterization of materials

NT-WO_3 and P25-WO_3 supports were characterized by inductively coupled plasma, BET surface area and pore volume using nitrogen adsorption-desorption isotherms at −196 °C. Their structural characterization (morphology and presence of TiO_2 phases in both supports) was performed employing X-ray diffraction (XRD) and transmission electron microscope (TEM); and the band-gap was determined by UV–Vis diffuse reflectance spectra. More details for the characterization of NT-WO_3 and P25-WO_3 can be found elsewhere [17]. The Pd content of the catalysts was analysed by ICP-OES: inductively coupled plasma with an Optical emission spectrophotometer (Spectro Arcos FHS-16). Total Pd content of the catalysts was determined by subtraction of the Pd content of the liquid sample before and after the metal deposition procedure. The BET surface area and pore volume of the photocatalysts were determined by nitrogen adsorption-desorption isotherms obtained at −195.85 °C using a Quadrasorb *SI* Models 4.0 using QuadraWin Software (v. 5.0+newer). Before the analysis, the samples were outgassed at 150 °C for 18 h under vacuum 6 milliTorr in the instrument pre-chamber to eliminate chemisorbed volatile species.

The crystalline phases present in the P25 and TiO_2-anatase photocatalysts were determined using a Bruker-AXS D8-Discover diffractometer with parallel incident beam (Göbel mirror) and vertical theta-theta goniometer, XYZ motorized stage mounted on an Eulerian cradle, diffracted-beam Soller Slits, a 0.2° receiving slit and a scintillation counter as a detector. The angular 2 theta diffraction range was between 20 and 70 °C. The data were collected with an angular step of 0.03° at 7 s per step. Cu_k radiation was obtained from a copper X-ray tube operated at 40 kV and 40 mA. Additionally, for the photocatalysts based on Pd, WO_3 and P25 or NT, the XRD measurements were also performed at an angular 2 theta diffraction range between 5 and 70° and the data were collected with an angular step of 0.05° at 3 s per step.

High resolution-transmission electron microscopy (HRTEM) analyses were carried out with a JEOL 2010F instrument equipped with a field emission source. The point-to-point resolution was 0.19 nm and the resolution between lines was 0.14 nm. The X-Ray photoelectron spectroscopy (XPS) data were acquired in a VG Escalab 200R electron spectrometer equipped with a hemispherical electron analyzer, operating in a constant pass energy mode, and a non-monochromatic Mg-*K*α (*hv* = 1253.6 eV, 1 eV = 1.603×10^{-19} J). X-ray source was operated at 10 mA and 1.2 kV. The angle of the incident photon beam was 45° with respect to the normal of the sample. The background pressure in the analysis chamber was kept below 7×10^{-9} mbar during data acquisition. The binding energy (BE C1s = 284.9 eV) of adventitious C1 was used as reference. A Shirley background subtraction was applied and Gaussian–Lorentzian product functions were used to approximate the line shapes of the fitting components.

BG values were determined from Tauc's plot, $(\text{energy} * \text{abs})^{1/2}$ vs. energy for indirect transition, obtained by diffuse reflectance UV–Vis of solids, measured by a UV-2410 PC spectrometer with integrating Sphere attachment (SHIMADZU ISR-240), converting it into absorbance using the Kubelka-Munk function $[\text{Photon energy} * \text{Absorbance}]^{1/2}$ versus the Photon energy and extrapolation to y = 0 of the linear regression. Samples consist of a mixture between powders from the semiconductor materials and barium sulfate ($BaSO_4$), as a standard.

Photocatalytic H_2 production

Firstly, photocatalytic H_2 production was studied at lab scale using two different reaction systems (Solar Simulated Light and UVA light system) with continuous stirring that have been detailed in our previous work [16]. Briefly, the solar box system consisted of a solar simulator chamber (SUNTEST CPS+) with a Xe lamp (300–800 nm; 250 W/m^2, $I_{250–450nm}$: 6.5×10^{-4} E/min). The UVA system consisted on a white methacrylate chamber equipped with four UVA lamps (300–400 nm; 15 W/lamp, $I_{250–450nm}$: 8.3×10^{-5} E/min). H_2 evolution was monitored by on-line gas chromatography (Shimadzu, GC-14B, Carbosieve SII column, TCD detector, carrier gas: Ar with flow rate of 25 ml/min).

In a typical photocatalytic experiment, the reactor was loaded with an aqueous solution of methanol or glycerol (5, 10, 25 or 50 vol%) and the catalyst (500, 333, 167 or 83 ppm, where ppm refers to mg/L). Then, the reactor was placed inside the irradiation box, and the solution was bubbled with Ar (50 ml/min) around 60 min to remove the air inside the reactor. The reactor remained under irradiation for 185 min and every 15 min a gas sample was automatically injected into the gas chromatograph for analysis. The number of incident photons on the reaction medium was measured by actinometry with the method based on the photochemical reduction of the ferrioxalate $[Fe(C_2O_4)_3]^{3-}$ complex to Fe(II) in acidic environment [[18], [19], [20], [21]].
Total organic carbon (TOC) and the pH of the mixtures before and after the reaction were followed up with a total organic carbon analyzer (Shimadzu TOC-L CSH/CSN) and a HANNA instrument (HI 5222). In real wastewater samples, chloride and conductivity were measured with an electrode ISE Chloride with a selective membrane: solid state $AgCl/Ag_2S$ (CRISON) and a CRISON 5061 conductivity cell, respectively.
In the second part of the work, photocatalytic H_2 production tests were carried out in a solar pilot plant at Plataforma Solar de Almería (PSA) (Spain). The system consisted in two sections (see Fig. 1): (i) a closed stainless steel tank of 27 L, provided with gas and liquid inlets and outlets, and a liquid sample port. A centrifugal pump (PanWorld NH-100PX) with a flow rate of 20 L/min was used to recirculate the aqueous solution from the tank to the tubes of the Compound Parabolic Collector (CPC); and (ii) a CPC photoreactor composed of 16 Pyrex glass tubes (inner diameter 28.45 mm, outer diameter 32.0 mm, length 1401 mm) mounted on a fixed platform tilted 37° (local latitude).

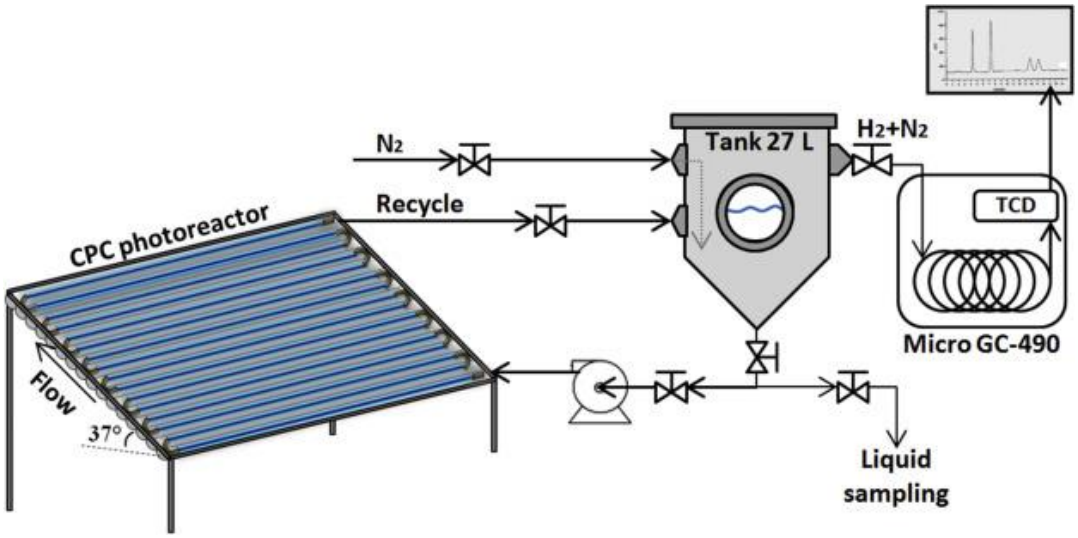

Fig. 1. Experimental set up of photocatalytic H_2 generation in the pilot-scale solar reactor.

The total irradiated area and volume were 2.1 m^2 and 14.25 L, respectively. In a typical experiment, the catalyst (5 g) was sonicated in water for 15 min, then, the tank was loaded with 25 L of an aqueous solution (0.2, 0.37 or 5 vol% of methanol or glycerol in water). The later solution was circulated through the system (from the tank toward the CPC photoreactor and again the tank) in the dark for 15 min and the tank was bubbled with N_2 for 10 min. After that, the CPC photoreactor was uncovered and left under solar irradiation around 6 h. Every 60 min a gas sample was manually injected into a gas micro-chromatograph (Agilent technologies 490, CP-MolSieve 5A column channel: 10 m

with backflush and retention time stability, TCD detector, carrier gas: N_2, injection and oven temperatures: 90 °C and 50 °C, respectively).
When solar radiation is used as an energy source it is necessary to take into account its lack of steadiness and the fact that it changes during the day or in 1 h (depending on the time and weather of the day, or the season). Therefore, in order to compare H_2 production of experiments performed in different days, it is required to normalize the data by using Eq. (1):(1)QUV,n=QUV,n−1+ΔtnUV¯G,nAiVtWhere QUV,n(kJ/L) is the solar UV energy accumulated per reactor volume unit along the experiment and it is used instead of the irradiation time so as to normalize the H_2 evolution. This irradiation is referred to the 300–400 nm wavelength range. Δtn(seg) is the experimental time for every gas sampling, Ai(m2) is the irradiated area of the CPC photoreactor, Vt(L) is the volume of the solution loaded to the tank and UV¯G,n(W/m2) is the average solar ultraviolet radiation intensity measured by a radiometer (KIPP&ZONNEN, CUV3 model) in the period Δtn. The radiometer provided data every minute of the incident radiation corresponding to wavelengths below 400 nm. The approximate value of QUV,n on the experimental days of autumn in Almería (around 10 h–16 h) is 30–35 kJ/L. Organic degradation was quantified as dissolved organic carbon (DOC) by using a Shimadzu VCSH TOC analyzer.

Results and discussion

Characterization of the photocatalysts

Some of the features of the characterization of photocatalytic materials used in this article are shown in Table 1. The objective was to study the influence of the metal deposition conditions on the photocatalytic H_2 evolution. Catalyst nomenclature includes the metal (Pd), the real Pd content (wt.%), Pd deposition method (wi or PD) and the Pd PD conditions (2m10, 2m5, 2m1, 4m10, 4w). Below Table 1, this nomenclature is detailed. Table 1 shows the amount of Pd determined by ICP-OES of the different samples. S_{BET}, V_{PORE} and BG energy (Eg) with its corresponding wavelength are also included in Table 1.

Table 1. List of catalysts used in this study and some of their features related to characterization of the solids.

Catalyst	Nominal Pd (wt.%)	Measured Pd % (ICP-OES)	E_g(eV)	λ_{max}(nm)	Particle size (nm) by TEM	S_{BET}(m^2g^{-1})	Total V_{PORE} (cm^3g^{-1})
Pd/NT-WO_3-2m10[a]	0.5	0.5	–	–	–	104.1	0.40
	0.25	0.21	2.89	429	1, 4 -10	99.6	0.34
	0.1	0.1	2.94	422	2–3	101.6	0.37
Pd/P25-WO_3-2m10	0.5	0.52	–	–	–	58.3	0.37
	0.25	0.23	2.99	415	2, 6 - 8	55.4	0.35
	0.1	0.1	3.00	414	<1	58.2	0.36
Pd/P25-2m10	0.5	0.51	3.00	414	4–12	56.6	0.41
	0.25	0.25	2.92	425	5–7	56.5	0.37
	0.1	0.09	2.94	422	<2	55.6	0.42
Pd/P25-2m5[b]	0.25	0.25	2.96	419	–	56.3	0.41
Pd/P25-2m1[c]	0.25	0.23	2.98	416	3–15	54.7	0.43

Catalyst	Nominal Pd (wt.%)	Measured Pd % (ICP-OES)	E_g(eV)	λ_{max}(nm)	Particle size (nm) by TEM	S_{BET}(m^2g^{-1})	Total V_{PORE} (cm^3g^{-1})
Pd/P25-WO_3-2m1	0.25	0.23	2.98	416	2, 4- 10	59.9	0.35
Pd/NT-WO_3-4m10[d]	0.25	0.26	2.96	419	–	101.4	0.37
Pd/P25-WO_3-4m10	0.25	0.27	3.00	414	–	59.7	0.35
Pd/P25-4m10	0.5	0.47	2.97	418	4–12	56.7	0.44
	0.25	0.21	2.95	421	5–7	55.7	0.36
	0.1	0.1	2.98	416	<2	54.9	0.43
Pd/NT-WO_3 -1m10[e]	0.25	0.15	2.94	422	–	100.5	0.33
Pd/NT-WO_3-4w[f]	0.25	0.013	2.94	422	<2	94.1	0.37
Pd/P25-WO_3-4w	0.25	0.011	3.06	406	<2	58.0	0.34
Pd/P25-4w	0.25	0.0092	3.08	403	5–7	55.2	0.40
Pd/P25-wi[g]	0.25	0.25	2.98	416	5–15	53.1	0.40
NT-WO_3	–	–	2.97	418	–	104.6	0.39
P25-WO_3	–	–	3.08	403	–	58.8	0.37
P25	–	–	3.10	399	–	54.7	0.26
TiO_2-anatasa	–	–	3.14	395	–	9.8	0.06

Pd deposition with:
[a] 2000 ppm of catalyst in a mixture of water-methanol (10 vol% methanol).
[b] 2000 ppm of catalyst in 5 vol% methanol.
[c] 2000 ppm of catalyst in 1 vol% methanol.
[d] 4000 ppm of catalyst in 10 vol% methanol.
[e] 1000 ppm of catalyst in 10 vol% methanol.
[f] 4000 ppm of catalyst in mlQ water.
[g] Wetness Impregnation.

Comparing the Pd content of the PD-m and PD-w methods, it is possible to see that, in those catalysts with Pd deposited by PD-m, the Pd content is above 80% of the nominal content, while by PD-w, the content of the Pd deposited was scarcely around 10%. This fact reveals the importance of a sacrificial agent in the PD methods, which acts as h^+ scavenger; therefore, more photoexcited e^- are available to reduce the Pd^{+2} in solution to Pd^0 on the semiconductor support surface.

Figure S1, of the supplementary information shows NT-WO_3, P25-WO_3 and P25 supports are mesoporous materials with type IV isotherms according to IUPAC [22]. More details about these three supports can be found in our previous work [16]. From physisorption analysis, specific area (S_{BET}) and pore volume (V_{PORE}) were estimated (Table 1). The deposition of 0.1 wt% of Pd by the PD 2m10 method reduces the S_{BET} and V_{PORE}, 104.6 m^2/g and 0.39 cm^3/g for NT-WO_3, and 101.6 m^2/g and 0.37 cm^3/g for Pd(0.1 wt%)/NT-WO_3, which could explain the hysteresis loop change observed in Figure S1 (a). On the other hand, increasing the Pd content beyond 0.1 up to 0.5 wt%, S_{BET} and V_{PORE} increase lightly, but not significantly. In the case of P25-WO_3 (Figure S1 (b)) and P25 (Figure S1 (c)) supports, they show similar S_{BET} after Pd

deposition. This is probably because the Pd nanoparticles (5–7 nm) are located outside the pores.

Fig. 2 shows the X-ray diffraction patterns for Pd/NT-WO_3, Pd/P25-WO_3 and Pd/P25 catalysts. All three supports exhibited similar diffraction lines referable to anatase phases (A) [16]. Regarding the effect of the PD method on the crystalline phases, in Fig. 2 is not seen important changes with the incorporation of Pd and peaks corresponding to Pd are neither detected. The absence of any signal of Pd species could suggest a very well dispersion of Pd in the support, containing very small nanoparticles, or might be in atomic size. In order to check some contribution of Pd to XRD patterns, additional XRD measurements were done for three catalysts with the highest Pd load. In Fig. 2, only the Pd(0.5 wt%)/NT-WO3 sample (Fig. 2 (a)) presents two peaks corresponding to Pd. These Pd peaks are not observed in Fig. 2(b)–(d), in the case of Pd(0.21 wt%)/NT-WO3 because of the lower Pd loading and in the case of Pd(0.52 wt%)/P25-WO3 and Pd(0.51 wt%)/P25 as a consequence of rutile phase with a reflection around 2θ = 39°.

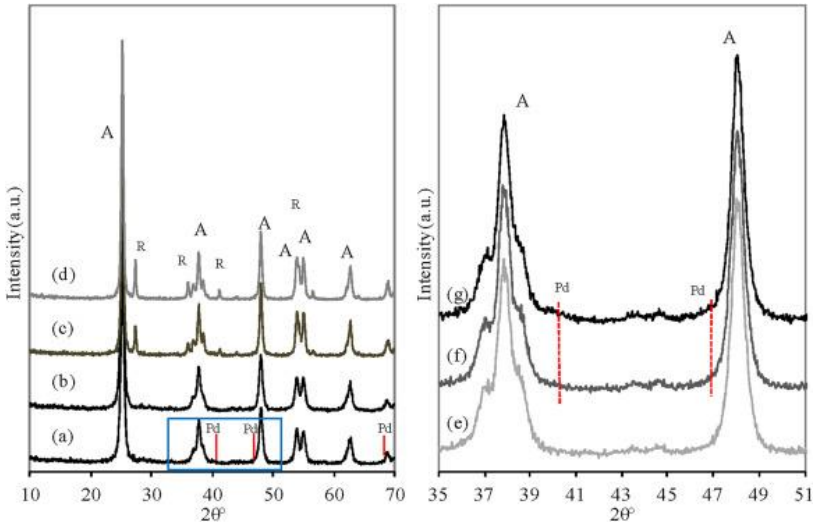

Fig. 2. XRD patterns. a) Pd(0.5 wt%)/NT-WO_3-2m10; b) Pd(0.21 wt)/NT-WO_3-2m10; c) Pd(0.52 wt%)/P25-WO_3-2m10; d) Pd(0.51 wt%)/P25-2m10; e) NT-WO_3; f) Pd(0.21 wt%)/NT-WO_3-2m10; g) Pd(0.35 wt%)/NT-WO_3-2m10.

Consequently, NT-WO_3, Pd(0.21 wt%)/NT-WO_3-2m10 and Pd(0.5 wt%)/NT-WO_3-2m10 samples were analysed again in order to enhance the signal/noise ratio from 35 to 51° 2θ, angular step of 0.03° at 12s per step. The results are shown in Fig. 2 (e), (f) and (g). It can be concluded that only for the highest Pd loading (0.5 wt%) is possible to see a small prominence of a peak corresponding to metallic Pd around 2θ = 40.1°. These XRD patterns may suggest that the low Pd loading results in very small Pd nanoparticles.

Fig. 3(a–d) shows representative STEM-HAADF (scanning transmission electron microscope - high-angle annular dark-field) images for Pd/P25 catalysts, where Pd was deposited under different PD conditions. It is possible to see that these samples are constituted by titania crystallites very well dispersed and quite homogeneous in size mostly in the range 20–30 nm. In addition, on the titania crystallites, there are brighter nanoparticles, which correspond to well dispersed Pd nanoparticles with about 5–7 nm in size. In the EDX spectrum included in Fig. 3 (a), it can be seen that there are signals of Ti and O arising from the titania support as well as Pd signals (the Cu signals are due to the copper grid used for TEM). Fig. 3 (d) shows a general STEM view of the sample prepared by 2m1, where a large number of Pd nanoparticles in the range 3–15 nm with a wide size distribution are displayed. The area enclosed by the white square in this

figure (Fig. 3 (d)) is shown in HRTEM mode in Fig. 3 (f). As expected, the bright nanoparticles in STEM mode show lattice fringes corresponding to Pd metal in HRTEM. Lattice fringes at 2.2 Å correspond to the (111) crystallographic planes of Pd in metallic Pd, and those at 3.6 Å correspond to the (101) crystallographic planes of anatase. There is no epitaxial relationship between titania and Pd nanoparticles.

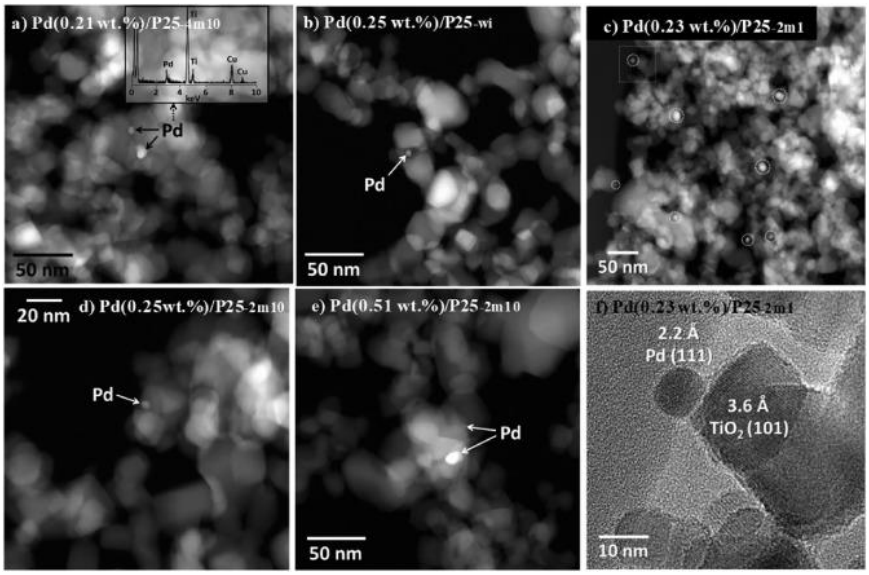

Fig. 3. STEM-HAADF images for Pd/P25 catalysts, where Pd was deposited by a) PD 4m10; b) wetness impregnation; c) PD 2m1; d) 2m10, e) PD 2m10, and f) 2m1.

From representative STEM-HAADF images for Pd/P25 catalysts with different amount of Pd (Fig. 3(d) and (e)), which were prepared by PD 2m10, the samples exhibited titania nanoparticles of 20–30 nm in size, Pd nanoparticles can be identified in the samples with 0.25 and 0.52 wt% of Pd, but they are not observed in the catalyst with 0.09 wt% Pd (not shown). This is likely due to the low Pd loading resulting in very small Pd nanoparticles that escape TEM detection. This fact can be deduced from Fig. 3(f) and (g), where the lower the Pd load (0.5 toward 0.25 wt%), the smaller the particle size (4–12 toward 5–7 nm, respectively).

Figure S2 shows TEM images for catalysts based on Pd/TiO_2-WO_3, where Pd was photodeposited. Sample Pd(0.21 wt%)/NT-WO_3 (smaller figure inside Figure S2 (a)) is constituted by two types of particles. Mainly it contains very small Pd nanoparticles of about 1 nm in diameter, but it also contains larger Pd particles from 4 up to 10 nm. An enlargement is shown in Figure S2 (a), where two particles of different size (1 and 4 nm) are marked inside black circles and a titania nanotube is clearly seen. EDX analysis shows that titania and WO_3 are intimate mixed. In all cases, signals of both Ti and W occur together and this is also observed in all the samples based on Pd/TiO_2-WO_3. Pd(0.23)/P25-WO_3-2m10 sample (Figure S2 (b)) is constituted mainly by Pd nanoparticles of 6–8 nm in diameter, but there are also a few nanoparticles measuring about 2 nm. Figure S2 (b) shows a representative STEM image with various Pd nanoparticles inside the white circles. The area enclosed in the white square is shown in the small image in Figure S2 (b) in HRTEM mode. A careful analysis of the lattice fringes demonstrates that the bright particles in the STEM mode do correspond to Pd nanoparticles. In HRTEM, Figure S2 (b), the lattice fringes measured at 2.2 Å correspond to the (111) crystallographic planes of metallic Pd, and the lattice fringes at 3.6 Å correspond to the (101) crystallographic planes of anatase.

Fig. 4 shows the surface chemical composition analysed by XPS for Pd/P25 catalysts. From the complete spectra for all the Pd/P25 catalysts, in Fig. 4 (a), the presence of O, Ti and C was verified with the O 1s, Ti 2p, C 1s and Ti 3p peaks at 531 eV, 460 eV, 285 eV and 38 eV, respectively. Regard to the Pd 3d XPS analysis (Fig. 5(b) and (c), (d)), for those Pd 3d signals that are well defined, in all cases Pd is oxidized at the surface. The binding energies recorded for Pd 3d 5/2 at around 336.7 eV and 341.9 eV are characteristic for Pd(II) species, which likely could be PdO or $Pd(OH)_2$ species [23].

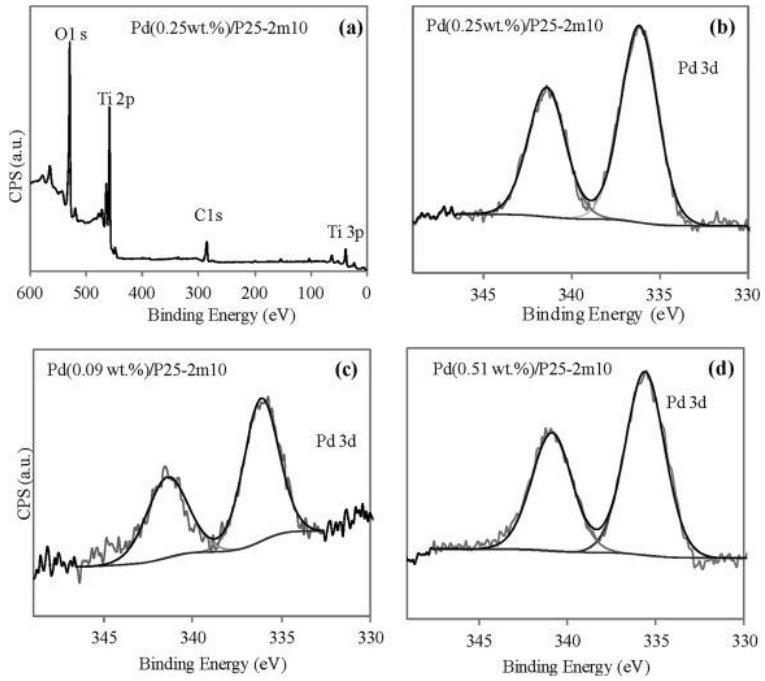

Fig. 4. XPS full spectra of the catalysts (a). High-resolution XPS spectra of Pd 3d (b,c, d) spectral region of Pd/P25 catalysts.

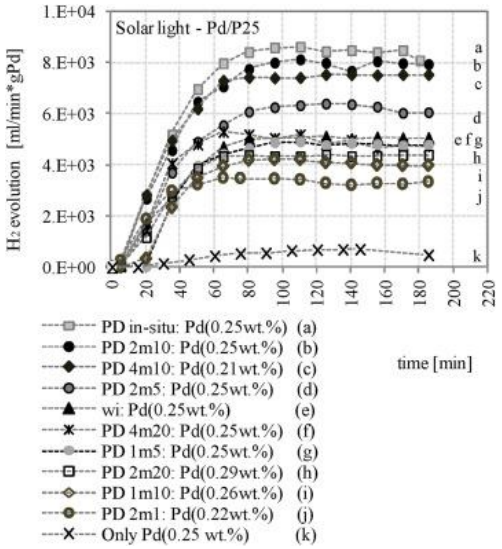

Fig. 5. H_2 generation for Pd/P25 varying the Pd deposition method. Experimental conditions: catalysts 167 ppm, 600 ml of a water-methanol (50 vol%) solution under simulated solar light (Xe Lamp, 300–800 nm, 250 W/m^2, $I_{250–450nm}$: 6.5 × 10^{-4} E/min.

The color of catalytic supports NT-WO_3, P25-WO_3 and P25 without Pd incorporated (Pd loading = 0 wt%) appeared whitish. When Pd is incorporated, either by PD-w or PD-m, or wi, the catalysts seem to turn into a grayish colour, lighter or darker depending on the amount of Pd loaded and the deposition method. This metallic appearance might be characteristic of the presence of metallic palladium Pd^0. Also, during the drying process at room temperature, most of the catalysts showed yellow traces, suggesting the oxidation of Pd while is drying, which could explain the initial time activation in photocatalytic experiments for H_2 production. This observation is in agreement with the Pd XPS results, where Pd as PdO or $Pd(OH)_2$ was observed.

BG energy values for all the catalysts are summarized in Table 1 together with the corresponding wavelength of absorption edge. From Table 1 it is possible to observe that the incorporation of Pd produces a slight decrease in the BG (Eg) and light absorption until higher wavelength for all the catalysts, even, for those whose Pd deposition was performed only in water. Some authors indicate that incorporating noble metals in semiconductor materials enhances light absorption towards the visible region, which can be attributed to a characteristic absorption of surface excitation due to plasmons of the metal nanoparticles [18,19]. The catalyst with the lowest BG energy and the highest wavelength absorption edge (2.89 eV, 429 nm) was Pd(0.21 wt%)/NT-WO_3-2m10. For Pd/P25 catalysts, the decreasing order of the band-gap value for the Pd deposition method is: PD-m > wi > PD-w.

H_2 production

In the present study, two types of h^+ scavenger sacrificial agents have been used. Methanol is the simplest alcohol, which can give an overview about the behavior of the new catalysts developed, Pd/TiO_2(WO_3), in this investigation, and also glycerol, to compare with a more complex molecule. In addition, a real wastewater containing a mixture of organic compounds has been tested in a pilot plant scale photoreactor to evaluate their activity under more realistic conditions. In order to understand the effect of Pd deposition on the H_2 evolution, the Pd amount (0.1, 0.25 and 0.5 wt%), catalyst concentration (1000, 2000 and 4000 ppm), sacrificial agent concentration (0, 1, 5 and 10 vol% methanol) and Pd addition time (in-situ and ex-situ) was varied. To clarify, Pd addition in-situ refers to the simultaneous addition of Pd in the photocatalytic H_2 generation reaction. Additionally, wi was studied for Pd/P25 catalysts. The quantum yield (QE or ϕ) (%) was calculated according to the literature as follows [20]:(2)ϕ=n(H2moleculesormed)unitimen(photonsexposed)unitime.100(%)

H_2 molecules formed are calculated from H_2 rate (mol/min.gCat) and *photons exposed* are determined by actinometrical data.

Effect of Pd deposition method

In Fig. 5 is shown the H_2 evolution on different Pd/P25 catalysts. In order to compare the catalytic activity of the Pd nanoparticles, H_2 evolution is presented per gram of Pd. Regarding the variation of the sacrificial agent concentration in the synthesis protocol (20, 10, 5 and 1 vol%), in Fig. 5 (b, d, h and j curves) is seen there is an optimal methanol concentration around 10 vol% in the PD, which leads to the highest H_2 evolution. This fact reveals the essential role of a sacrificial agent in the Pd PD, which may be related to the Pd nanoparticles size in agreement with TEM images of Pd/P25 (Fig. 3 (d) and (c)) -PD 2m1 method produces larger Pd nanoparticles than PD 2m10 method-.

Comparing the catalysts prepared at the same methanol concentration but different support concentration, Fig. 5(b and c and i curves), the slightly higher H_2 evolution for PD 2m10 (8120 ml/min.gPd) than 4m10 (7520 ml/min.gPd) methods could probably correspond to the smaller BG energy of the catalyst prepared by PD 2m10 method (2.92 vs. 2.95 eV). TEM images (Fig. 3 (a and d) corroborate that for both samples there are not obvious differences in the structure of the catalysts that make one catalyst better than the other one. Comparing PD 2m10 to PD 2m1 method, though they have similar amount of Pd deposited, 2m10 catalyst is more active. These results could be related to

the nanoparticles size. In Fig. 3(d), the PD 2m1 method shows Pd nanoparticles in the range of 3–15 nm in size. Although high methanol concentration in PD methods could cause larger metal particles [21,24], in the case of the catalysts prepared under low methanol concentration, initial Pd nanoparticles deposited could act themselves as active sites, therefore, even if the sacrificial agent concentration is low, this fact stimulates further Pd growth and as a result Pd nanoparticles are larger in size.

Regarding to the catalyst prepared by wi (Fig. 5 (e curve)), its lower H_2 evolution compared to catalysts with the same amount of Pd (PD 2m10 or PD 2m5 method) can be explained by the greater Pd nanoparticles size (Fig. 3 (b)). Bowker et al. [25] explained that the active sites of metal nanoparticles for the formation of the e^-/h^+ pairs are placed around the edges of the metallic surface, where there is contact with the surface of the semiconductor support. Therefore, to increase the formation of e^-/h^+ pairs and consequently the H_2 generation, it is necessary to maximize that contact zone, which is possible with smaller nanoparticles size. Some other authors [[26], [27], [28]] agree on the fact that higher activity is possible by increasing the interaction surface between support and metal, which means deposit smaller metal nanoparticles on the catalytic support surface. From these results, we can range the Pd deposition methods, starting the highest H_2 generation toward the lowest one: PD in-situ, PD 2m10, PD 4m10, PD 2m5, wi, PD 4m20, PD 1m5, PD 2m20, PD 1m10 and PD 2m1, and their quantum efficiencies in decreasing order are: 14.5, 13.3, 10.7, 10.7, 8.7, 8.4, 8.2, 7.3 and 5%, respectively.

Concerning the induction period observed in Fig. 5, it could correspond to the photocatalytic reduction time of an oxidized form of the metallic-co-catalyst toward its reduced form ($M^+ \rightarrow M^0$, M: metallic element) [2,24,29,30]. Before irradiation, the Pd on the catalyst is oxidized (in agreement with the XPS results). Under irradiation, Pd is progressively reduced by the photoexcited e^-. In time, more e^- are photogenerated and more metallic Pd is formed (Pd^0), consequently more H^+ ions are adsorbed on Pd surface, increasing the H_2 evolution up to reaching the plateau observed in almost all the catalysts in this study.

Effect of the amount of Pd

The effect of the amount of Pd in H_2 production was studied varying the amount of Pd from 0 to 0.5 wt%. Fig. 6 suggests, for the three Pd/P25, Pd/NT-WO_3 and Pd/P25-WO_3 catalysts, an optimal amount of Pd photodeposited around 0.25 wt%.

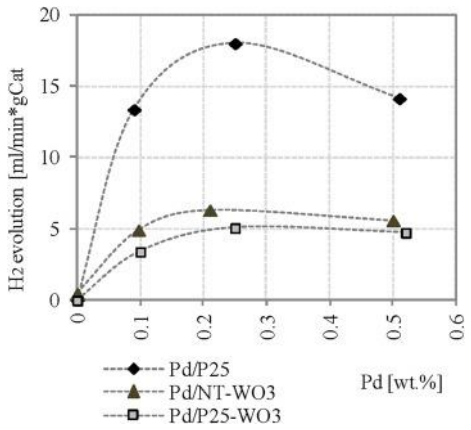

Fig. 6. H_2 evolution vs. Pd (wt.%) for Pd/P25, Pd/NT-WO_3 and Pd/P25-WO_3 catalysts, varying the amount of Pd deposited. Experimental conditions: catalysts 166.67 ppm, 600 ml of a water-methanol (50 vol%) solution under simulated solar light (Xe Lamp, 300–800 nm, 250 W/m^2, $I_{250-450nm}$: 6.5×10^{-4} E/min). Pd incorporation by PD-2m10.

The supports without Pd present very low H_2 evolution (0.03, 0.5 and 0.003 ml/min.gCat, respectively). When 0.1 wt% of Pd is incorporated, the H_2 evolution increased up to a plateau of 13.37, 4.92 and 3.41 ml/min.gCat for Pd/P25, Pd/NT-WO_3 and Pd/P25-WO_3, respectively. Once Pd content increased up to 0.25 wt%, the H_2 evolution increased as well (18, 6.33 and 5.08 ml/min.gCat). However, when the Pd is increased to 0.5 wt%, a decrease was observed in the H_2 evolution (14.14, 5.69 and 4.74 ml/min.gCat). This optimal load of Pd -in the range studied-might means that for lower amount of Pd, the metal quantity is deficient to avoid e^-/h^+ recombination and at higher Pd loading, the Pd dispersion gets worse. Accordingly, in both cases, the H_2 evolution decreases. Some authors explained that for a too high metal content, the catalytic support could be extremely covered, therefore the light absorption is decreased [15,31].

Pilot plant testing

For H_2 tests in the pilot plant installation, accordingly to previous work [7,8], the optimal catalyst loading and reaction volume were 200 ppm and 25 L, respectively. In this experimental set was used aqueous solutions of methanol (0.2, 0.37 and 5 vol%), glycerol (0.37 and 5 vol%) and municipal wastewater under solar light around 6 h. All the catalysts tested were prepared by PD 2m10 method. H_2 evolution vs. accumulated solar UV energy per reactor volume unit, (Q (kJ/L)), in water-methanol or water-glycerol solutions is presented in Fig. 7 (a). The accumulated solar UV energy was described in Eq. (1). Each point corresponds to every hour of irradiation. In this figure, it is seen three concentrations of methanol or glycerol (5, 0.37 and 0.2 vol%) for Pd/P25 catalyst and 0.37 vol% for both Pd/TiO_2-WO_3 based catalysts.

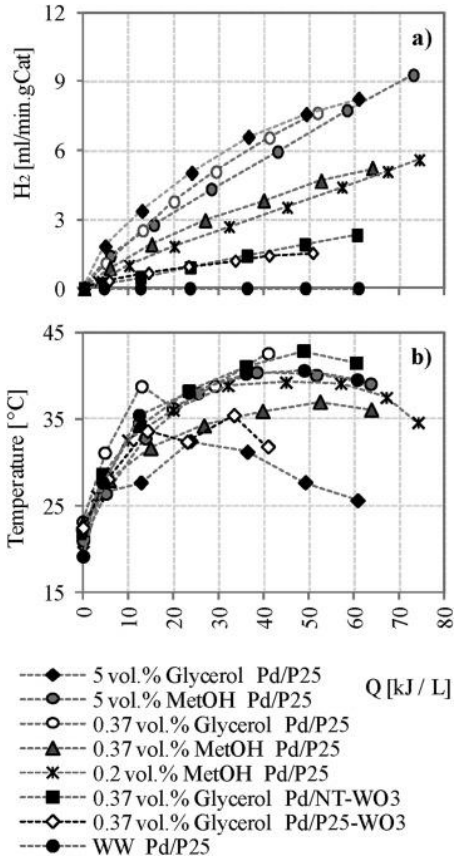

Fig. 7. H_2 evolution vs. accumulated solar UV energy for Pd (0.25 wt%)/P25 in water-methanol and -glycerol mixtures. Experimental conditions: catalysts 200 ppm in 25 L under solar light. WW: municipal wastewater from Almería, Spain.

Comparing the effect of methanol concentration, the higher it is, the higher the H_2 generation. Regarding the H_2 evolution at 0.37 vol% glycerol and methanol, Pd/P25 showed the highest H_2 evolution (7.6 and 5.2 ml/min.gCat) after 6 h of reaction, followed by Pd/NT-WO_3 and Pd/P25-WO_3 (2.3 and 1.5 ml/min.gCat, respectively) in glycerol. For tests with 5 vol%, Pd/P25 showed higher H_2 evolution in methanol than glycerol at the end of the reaction (9.3 and 8.2 ml/min.gCat). This fact could be explained looking at Fig. 7 (b), which shows the temperature profile of the gas phase of the reactor vs. Q (kJ/L). It is possible to see that for the test at 5 vol% glycerol, the temperature starts to decrease after 15 kJ/L, and comparing to the H_2 evolution (Fig. 7 (a)), ca. at the same moment, it also decreases.

Concerning the H_2 evolution when municipal wastewater (WW) was used, it scarcely reached 0.003 ml/min.gCat. Table S1 in Supplementary Information shows the main physicochemical characteristics of the municipal wastewater, before and after the reaction. The low H_2 evolution using wastewater as source of e^- donors is understandable due to the presence of different species that can poison the catalyst surface by adsorption (metals, ions, etc.) [[32], [33], [34]]. These results demonstrate the challenges to overcome the photocatalytic H_2 generation by using municipal wastewater from a secondary treatment, that is mainly affected by the high concentration of impurities, which can be compounds that either, compete with the generation of H_2 or deactivate the catalyst by adsorption.

Comparing these results to previous ones achieved by different catalysts based on noble metal (Pd, Pt or Au) supported on TiO_2 performed in the same pilot plant using different sacrificial agents [7,8] (Table S2), the result of the ϕ for Pd(0.25 wt%)/P25-2m10 catalyst seems to be good enough compared to Au (0.5 wt%)/TiO_2 catalyst: 2.37 vs. 2.34% in glycerol and 1.33 vs. 0.21% in methanol, respectively, if we take into account the lower metal loading. On the other hand, though the fact that the efficiencies of both catalysts, Pd/NT-WO_3 and Pd/P25-WO_3, appear still low (0.57 and 0.47%, respectively), it is important to highlight that in the literature, the amount of noble metal deposited is higher, 0.5 and 2 wt % vs. 0.25 wt% in the present study.

Quantum efficiencies and literature comparison

Table 2 shows a summary of the different catalysts studied under UVA and solar simulated irradiation, respectively, and Table 3 presents a comparison of ϕ for H_2 production for different photocatalytic materials.

Table 2. Quantum yields of catalyst prepared in this study.

Catalyst	**Light**	**Weight % (ICP-OES)**	**Total volume of H_2 [ml]**	**Rate H_2 [mol/min.gCat]**	**H_2 [ml/min.gCat][b]**	**Quantum Yield ϕ (%)[a]**
Pd/P25-2m10	UV light[a]	0.25	185	8.6 × 10-4	19.2 ± 3.7	41.2
Pd/NT-WO_3 -2m10		0.21	125	3.7 × 10-4	8.4 ± 0.6	18.8
Pd/P25-WO_3-2m10		0.23	67	1.9 × 10-4	4.2 ± 0.6	9.9
Pd/P25-2m10	Solar simulated light[b]	0.25	284	8.0 × 10-4	17.9 ± 1.9	11.8
Pd/P25-2m5		0.25	241	7.1 × 10-4	16 ± 1.4	11
Pd/P25-4m10		0.21	232	6.8 × 10-4	15.2 ± 1.5	10.4

Catalyst	Light	Weight % (ICP-OES)	Total volume of H_2 [ml]	Rate H_2 [mol/min.gCat]	H_2 [ml/min.gCat][b]	Quantum Yieldϕ (%)[a]
Pd/P25-wi		0.25	171	4.9 × 10-4	11 ± 1.8	7.6
Pd/P25-2m10		0.09	181	5.3 × 10-4	11.8 ± 1.6	8.3
Pd/P25-2m10		0.51	164	5.2 × 10-4	11.6 ± 2.3	8.0
Pd/P25-2m1		0.23	156	4.4 × 10-4	9.8 ± 1.9	6.7
Pd/NT-WO_3-2m10		0.21	101.4	2.8 × 10-4	6.3 ± 0.5	4.1
Pd/NT-WO_3-4m10		0.26	94	2.8 × 10-4	6.2 ± 0.6	4.1
Pd/NT-WO_3 -1m10		0.15	94	2.9 × 10-4	6.5 ± 0.9	3.9
Pd/P25-WO_3-4m10		0.27	74	2.4 × 10-4	5.3 ± 0.4	3.6
Pd/P25-WO_3-2m10		0.23	73	2.4 × 10-4	5.3 ± 0.7	3.4
Pd/P25-WO_3-2m1		0.23	62	2.1 × 10-4	4.7 ± 0.6	3.4

The uncertainty was estimated taking into account the repeatability, resolution and accuracy equipment and calibration curve.

[a] Experimental Conditions: catalysts 166.67 ppm, 250 ml of a water-methanol (50 vol%) solution under simulated UVA light (300–400 nm; 4 lamps of 15 W/lamp, $I_{250–450\ nm}$: 8.3 × 10^{-5} E/min). Irradiation time: 3 h
[a] Experimental Conditions: catalysts 166.67 ppm, 600 ml of a water-methanol (50 vol%) solution under simulated solar light (Xe Lamp, 300–800 nm, 250 W/m^2, 65e^{-4} E/min). Irradiation time: 3 h

Table 3. Comparison of quantum yield for H_2 production[a] for different photocatalytic materials.

Catalyst	Irradiation	Sacrificial Agent	Rate H_2 [mol/min.gCat]	Quantum YieldΦ (%)[a]
Pt(0.5 wt%)/TiO_2 [40]	Visible	0.01 vol% $ClCH_2COOH$ in 0.1 L	5.6 × 10-6	2.33
			1.5 × 10-6	0.62
Pt(0.5 wt%/CdS(50%)-TiO_2/FTO	Monochromatic light (470 nm)	20 vol% EtOH in 0.1 L	–	20
Pt(0.5 wt%/CdS(50 mol%)-TiO_2 [9]	Solar simulated	Na_2SO_3; Na_2S 0.007 M; 0.0048 M in 0.06 L	1.1 × 10-5 (r_{max})	2.7
1 wt%$Pd_{shell}Au_{core}/TiO_2$ [41]	UV LED (365 nm)	25 vol% Glycerol in 0.025 L	3.3 × 10-4	37.63
Pt(0.5 wt%)/TiO_2 DP	UV	10 vol% Pronan-2-ol in 0.085 L	1.1 × 10-3	13.3
Pt(1.5 wt%)/TiO_2 DP			1.1 × 10-3	13.3
Pt(0.5 wt%)/TiO_2 IMP			1.2 × 10-3	13.5
Pd(0.5 wt%)/TiO_2 DP [15]			1.1 × 10-3	13.3
Pd(1 wt%)/TiO_2	Solar	100 vol% EtOH (0.1 L)	5.5 × 10-5	10
Pt(1 wt%)/TiO_2			5 × 10-5	10

Catalyst	Irradiation	Sacrificial Agent	Rate H_2 [mol/min.gCat]	Quantum Yield Φ (%)[a]
Rh(1 wt%)/TiO_2 [20]			2 × 10-5	4
Pt(0.5 wt%)/TiO_2 [42]	Solar	0.003 vol% (0.85 mM) MetOH	4.6 × 10-6	0.47
	Solar	0.005 vol% (0.86 mM) EtOH	9.5 × 10-6	0.97
	Solar	52 vol% (8.91 M) EtOH	8.7 × 10-5	8.97
	UV	3.3 vol% (0.57 M) EtOH in 0.06 L	4.5 × 10-4 (r_{max})	17.14
Film Pt/TiO_2 [43]	Black light 365 nm	80 vol% EtOH	1.8 × 10-4	36.4
		80 vol% MetOH	1.5 × 10-4	30.1
		40 vol% EtOH	1.5 × 10-4	29.4
		40 vol% MetOH in 0.09 L	1.1 × 10.4	22.4
Pt(1 wt%)-$BaTi_4O_9$ [44]	UV	20 vol% EtOH in 0.1 L	2.4 × 10-4	5.9
Pt(0.1 wt%)/$SrTiO_3$:Rh(1%) [29]	420 nm	10 vol% MetOH in 0.15 L	9.6 × 10-7	2.6
$NaTaO_3$	UV 254 nm	Water splitting in 0.2 L	3.5 × 10-6	1
Au–Pd (0.95 wt%)/$NaTaO_3$ [45]			2.8 × 10-5	6.5
NiO(0.2 wt%)/$NaTaO_3$:La(2 mol%) [39]	270 nm	Water splitting in 0.3 L	3.3 × 10-4	28
Pd(0.5 wt%)/TiO_2	UV 365 nm	10 vol% Glycerol	6.9 × 10-4 (1)	–
		10 vol% 1,2-ethanediol	5.78 × 10-4 (2)	–
Pd(1 wt%)/TiO_2 [46]		10 vol % 1,2-propanediol	7.9 × 10-4 (1)	–
		10 vol% Glycerol in 0.2 L	7.41 × 10-4 (2)	–
Pd(0.5 wt%)/TiO_2 [47]	Solar spectrum	0.5 vol% MetOH	2.7 × 10-5	–
		1.7 vol% Triethanolamine	5.7 × 10-5	–
Pd(0.3 wt%)/TiO_2 [48]	400 W Xenon arc lamp	0.1 vol% Ag. in 100 ml	–	–
Pd(0.1 mol%)/TiO_2 [49]	UV 365 nm	50 vol% MetOH	4.1 × 10-7	–
Pt(0.5 wt%)/P25 [50]	280–650 nm	10 vol% (2.48 M) MetOH in 15 ml	5.5 × 10-6	5.5% (AQE)
Pt/TiO_2–N	Solar	0.37 vol% (0.05 M) Glycerol in 25 L	5.5 × 10-5	3.2
Pt/CdS–ZnS [7]			3.5 × 10-5	2

[a] Quantum yield [20,41,43].

Regarding the results under UVA light in this paper, the catalyst with the maximum ϕ was Pd(0.25 wt%)/P25 with 41.2% (Table 2) in 185 min. On the other side, although ϕ of Pd/NT-WO_3 and Pd/P25-WO_3 catalysts were only near to 20 and 10% (Table 2), compared to the literature (Table 3), they still seem to be promising under UVA light.

With regard to solar light, the H_2 evolution for most of the Pd/P25 catalysts were higher than all those catalysts with the WO_3 incorporated. The Pd PD in-situ method (see also Fig. 5) lead to the highest ϕ for every kind of catalyst: 14.5, 4.9 and 4.7% for Pd/P25, Pd/NT-WO_3 and Pd/P25-WO_3, respectively. Following, the catalysts prepared by PD 2m10 method were the second best: 11.8, 4.1 and 3.4% respectively. On the other side, the lowest ϕ were 3.9 and 2.8% for Pd/TiO_2-WO_3 catalysts prepared by PD 1m10 and PD 2m1 method, respectively. It reflects the fact that the preparation conditions have important effects on the final catalytic activity of any material [24,26,28,35,36], which, in this study, was observed in the Pd deposition and such differences are related, not only to the method efficiency to deposit the nominal metal amount, but also with the dispersion and metal nanoparticles size and their interaction with the catalytic supports, as was seen for Pd/P25 and Pd/TiO_2-WO_3 catalysts. So as to clarify this point, in Fig. 8 is presented the effect of Pd nanoparticles size on the ϕ of various Pd/P25 catalysts.

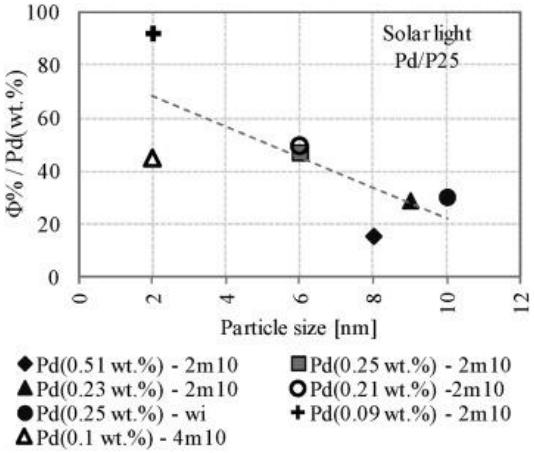

Fig. 8. Effect of Pd particle size on quantum yield (Φ %/Pd(wt.%)) for different Pd/P25 catalysts. Experimental conditions: catalysts 166.67 ppm, 600 ml of a water-methanol (50 vol%) solution under simulated solar light (Xe Lamp, 300–800 nm, 250 W/m^2, $I_{250–450nm}$: 6.5 × 10^{-4} E/min).

As these catalysts contain different amount of Pd, in order to make an appropriate comparison between all of them, the ϕ values are normalized taking into account the content of Pd (wt.%). Then, in Fig. 8 is presented the ϕ per content of Pd, ϕ %/Pd(wt.%), versus Pd particle size. Dashed line shows the decreasing trend of this normalized quantum yield when Pd nanoparticle size increase. These results allow us to confirm that, the PD of smaller metal nanoparticles promote an improvement on the photocatalytic activity, not only toward H_2 production [27,37], but also to the sacrificial agent oxidation [26,28,38]; the smaller the metal particle size, the higher the surface area -to- volume ratio-where reactants are exposed to reaction [[26], [27], [28],[37], [38], [39]]. Therefore, considering that the H_2 generation on photocatalytic materials begins from the e^-/h^+ pair separation, it is understandable to consider the fact that, the higher the number of h^+ trapped by the sacrificial agent -organic compounds oxidation-, the higher the number of e^- available for H_2 generation, therefore, the higher the ϕ.

Fig. 9 shows the effect of the sacrificial agent -in the Pd photodeposition-on ϕ for different Pd/P25 catalysts, where Pd was photodeposited using different methanol concentration (20, 10, 5 and 1 vol%). Similar to Fig. 8, the ϕ was normalized per content of Pd (wt.%). From results in Fig. 9, it is possible to see an improvement of the normalized quantum yield for higher concentration of methanol in the Pd photodeposition, moreover, it is only applicable inside the range 1–10 vol% of methanol

in the Pd PD step. When the Pd PD was performed using 20 vol% of methanol, ϕ/Pd(wt.%) was much lower. Probably, a higher concentration of methanol (upper than 10 vol%) in the Pd PD causes larger metal particles [21,36].

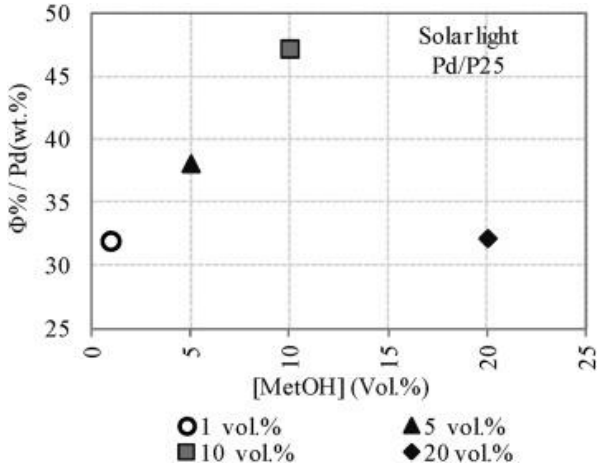

Fig. 9. Effect of methanol concentration -in the Pd photodeposition-on quantum yield (Φ %/Pd(wt.%)) for different Pd(0.25 wt%)/P25 catalysts. Experimental conditions: catalysts 166.67 ppm, 600 ml of a water-methanol (50 vol%) solution under simulated solar light (Xe Lamp, 300–800 nm, 250 W/m^2, $I_{250–450nm}$: 6.5 × 10^{-4} E/min). Pd incorporation by PD-2mX.

Table 3 shows the ϕ of different catalysts tested and published in the available literature, based most of them, on noble metal (Pd, Rh or Pt) supported on TiO_2, and the reactions carried out in aqueous solutions of different alcohols such as methanol, ethanol, propanol or glycerol. Looking at Table 3, in the case of Pt based catalysts under UVA light, the maximum ϕ was 36.4% [43] in around 250 min of reaction (however, there is not information about the amount of Pt deposited). Patsoura et al. [42] obtained a ϕ of 17.14% with the catalyst Pd(0.5 wt%)/TiO_2 in 60 ml of a water-ethanol solution (around 13 vol%) in 250 min [42]. Using a different kind of alcohol, Tenllado et al. [15] reached 13.5 and 13.3% of ϕ working with an aqueous solution of propanol (10 vol%) and 0.5 wt% of Pt impregnated and photodeposited on TiO_2, respectively.

Concerning the literature comparison under solar light, from Table 3 it can be seen that Yang et al. [20] have obtained the highest ϕ (10%) with Pt(1 wt%)/TiO_2 and Pd(1 wt%)/TiO_2 catalysts in 100 ml of ethanol, and Patsoura et al. [42] reached 8.97% with Pd(0.5 wt%)/TiO_2 in 60 ml of a water-methanol solutions. Regarding the results of the ϕ under solar light, the catalysts studied in this paper seem to be promising, not only because some of their ϕ are higher than the literature values, but also, because the amount of metal deposited on most of the supports is between 0.1 and 0.25 wt%; it means, lower noble metal, so this factor might become our competitive point, if we take into account the high price of some precious metal (1505.90 €/oz for Au, 995.86 €/oz for Pt and 2349.05 €/oz for Pd, according to the informative prices from the London market (LBMA) consulted on 13/05/, 2021, at 18.30 h Spanish time).

Conclusions

H_2 generation from aqueous solution of glycerol and methanol, and also from wastewater has been studied on a series of Pd/TiO_2(-WO_3) based catalysts. It was observed that the introduction of Pd on all the bare supports produced a strong increase in the rate of H_2 generation. The results suggested an optimal Pd loading of 0.25 wt%. With regard to the photodeposition conditions, it was found, for the three supports, P25, NT-WO_3 and P25-WO_3, that both, methanol and catalyst concentration, seem to have an

optimal value -inside the range studied-at around 10 vol% methanol and 2000 ppm for the catalytic support (PD 2m10 method).
The photodeposition conditions influence on the Pd nanoparticle size, where the smaller nanoparticles were observed for all those catalysts containing the lowest content of Pd (0.1 wt%) and larger for the highest content of Pd (0.5 wt%).
Concerning the differences between the lower H_2 generation on both Pd/TiO_2-WO_3 based catalysts compared to Pd/P25, it was considered that it could be probably due to the incorporation of WO_3, which lead to produce secondary products that can deposit on the catalyst surface, obstructing the hydrogen ions adsorption, therefore the H_2 evolution. With regard to the better TOC removal results but worse H_2 generation under solar light than under UVA light, this could be an indication of a competitive electron trapping between H ions and O2: when the H ions adsorption prevail, the H_2 generation is favored meanwhile the degradation of organic compound get worse; on the other hand, when O2 adsorption prevails, there is a higher TOC removal while the H_2 evolution is lower.
For H_2 tests at large scale, the three families of catalysts were able to produce H_2 in a pilot-scale solar Compound Parabolic Collector (CPC) at the Solar Platform of Almeria from water-methanol (0.2, 0.37 and 5 vol%) and glycerol (0.37 and 5 vol%) mixtures. For all H_2 tests in this set, Pd/P25 catalysts showed the highest H_2 evolution compared to Pd/TiO_2-WO_3 based catalysts. At 0.37 vol% glycerol and methanol on Pd/P25, H_2 evolution was 7.6 and 5.2 ml/min.gCat, respectively, and on Pd/NT-WO_3 and Pd/P25-WO_3 the H_2 evolution was 2.3 and 1.5 ml/min.gCat, respectively, in glycerol.
For tests at 5 vol% in the solar box, Pd/P25 showed highest H_2 evolution in glycerol than methanol (10.3 and 6.9 ml/min.gCat). Although glycerol is a more complex molecule than methanol, likely the higher oxidation state of its two methyl carbons than the unique methyl carbon in methanol, make glycerol possible to be oxidized easierly. With municipal wastewater was found a very low catalytic activity (0.003 ml/min.gCat), which is probably caused by high amount of impurities, such as dissolved inorganic solids or heavy metals. The highest H_2 evolution in this paper under both UVA and solar light was obtained by Pd(0.25 wt%)/P25-2m10, 19.2 ± 3.7 (ϕ: 41.2%) and 17.9 ± 1.9 ml/min.gCat (ϕ: 11.8%) at lab-scale, respectively. Pd(0.21 wt%)/NT-WO_3 and Pd(0.23 wt%)/P25-WO_3 catalysts produced 8.8 ± 0.6 (ϕ: 18.8%) and 4.2 ± 0.6 ml/min.gCat (ϕ: 9.9%) under UVA light, and under solar light they were 6.3 ± 0.5 (ϕ: 4.1%) and 5.3 ± 0.7 (ϕ: 3.4%), respectively.

Acknowledgments

This work is being supported by the Spanish Ministerio de Economía y Competitividad (MINECO) through the project CTQ2012-37039-C02-02, CTM2015-71054-REDT (FOTOCAT) and ENE2015-63969-R.

References

A. Fujishima, K. Honda
TiO_2 photoelectrochemistry and photocatalysis
Nature, 213 (1972), p. 8656

W.T. Chen, A. Chan, D. SunWaterhouse, T. Moriga, H. Idriss, G.I.N. Waterhouse
Ni/TiO_2: a promising low-cost photocatalytic system for solar H_2 production from ethanol–water mixtures
J Catal, 326 (2015), pp. 43-53, 10.1016/j.jcat.2015.03.008

É. Karácsonyi, L. Baia, a. Dombi, V. Danciu, K. Mogyorósi, L.C. Pop, G. Kovács, V. Co şoveanu, A. Vulpoi, S. Simon, Z. Pap

The photocatalytic activity of TiO_2/WO_3/noble metal (Au or Pt) nanoarchitectures obtained by selective photodeposition
Catal Today, 208 (2013), pp. 19-27, 10.1016/j.cattod.2012.09.038

I. Dincer, C. Acar
Review and evaluation of hydrogen production methods for better sustainability
Int J Hydrogen Energy (2015), 10.1016/j.ijhydene.2014.12.035

A. Kudo, Y. Miseki
Heterogeneous photocatalyst materials for water splitting
Chem Soc Rev, 38 (2009), pp. 253-278, 10.1039/b800489g

K. Maeda, D. Lu, K. Domen
Direct water splitting into hydrogen and oxygen under visible light by using modified TaOn photocatalysts with d^0 electronic configuration
Chem - A Eur J, 19 (2013), pp. 4986-4991, 10.1002/chem.201300158

K. Villa, X. Domènech, S. Malato, M.I. Maldonado, J. Peral
Heterogeneous photocatalytic hydrogen generation in a solar pilot plant
Int J Hydrogen Energy, 38 (2013), pp. 12718-12724, 10.1016/j.ijhydene.2013.07.046

S.Y. Arzate,Salgado, R.M. Ramírez,
Zamora, R. Zanella, J. Peral, S. Malato, M.I. Maldonado
Photocatalytic hydrogen production in a solar pilot plant using a Au/TiO_2 photo catalyst
Int J Hydrogen Energy, 41 (2016), pp. 11933-11940, 10.1016/j.ijhydene.2016.05.039

V.M. Daskalaki, M. Antoniadou, G. Li Puma, D.I. Kondarides, P. Lianos
Solar light-responsive Pt/CdS/TiO_2 photocatalysts for hydrogen production and simultaneous degradation of inorganic or organic sacrificial agents in wastewater
Environ Sci Technol, 44 (2010), pp. 7200-7205, 10.1021/es9038962

Y. Li, G. Lu, S. Li
Photocatalytic transformation of rhodamine B and its effect on hydrogen evolution over Pt/TiO_2 in the presence of electron donors
J Photochem Photobiol A Chem, 152 (2002), pp. 219-228, 10.1016/S1010-6030(02)00210-1

A. Patsoura, D.I. Kondarides, X.E. Verykios
Enhancement of photoinduced hydrogen production from irradiated Pt/TiO_2 suspensions with simultaneous degradation of azo-dyes
Appl Catal B Environ, 64 (2006), pp. 171-179, 10.1016/j.apcatb.2005.11.015

M. De Oliveira Melo, L.A. Silva
Photocatalytic production of hydrogen: an innovative use for biomass derivatives
J Braz Chem Soc, 22 (2011), pp. 1399-1406, 10.1590/S0103-50532011000800002

H. Zhou, J. Pan, L. Ding, Y. Tang, J. Ding, Q. Guo, T. Fan, D. Zhang
Biomass-derived hierarchical porous CdS/M/TiO_2 (M = Au, Ag, pt, pd) ternary heterojunctions for photocatalytic hydrogen evolution
Int J Hydrogen Energy, 39 (2014), pp. 16293-16301, 10.1016/j.ijhydene.2014.08.032

M.I. Badawy, M.Y. Ghaly, M.E.M. Ali
Photocatalytic hydrogen production over nanostructured mesoporous titania from olive mill wastewater
Desalination, 267 (2011), pp. 250-255, 10.1016/j.desal.2010.09.035

F.J. López-Tenllado, J. Hidalgo-
Carrillo, V. Montes, A. Marinas, F.J. Urbano, J.M. Marinas, L. Ilieva, T. Tabakova, F. R eid
A comparative study of hydrogen photocatalytic production from glycerol and propan-2-ol on M/TiO_2 systems (M=Au, Pt, Pd)
Catal Today, 280 (2017), pp. 58-64, 10.1016/j.cattod.2016.05.009

S.Y. Toledo,Camacho, A. Rey, M.D. Hernández,Alonso, J. Llorca, F. Medina, S. Contre ras
Pd/TiO_2-WO_3photocatalysts for hydrogen generation from water-methanol mixtures
Appl Surf Sci, 455 (2018), pp. 570-580, 10.1016/j.apsusc.2018.05.122

A. Rey, P. García-Muñoz, M.D. Hernández-Alonso, E. Mena, S. García-Rodríguez, F.J. Beltrán
WO_3-TiO_2 based catalysts for the simulated solar radiation assisted photocatalytic ozonation of emerging contaminants in a municipal wastewater treatment plant effluent
Appl Catal B Environ, 154–155 (2014), pp. 274-284, 10.1016/j.apcatb.2014.02.035

M. Shibuya, M. Miyauchi
Site-selective deposition of metal nanoparticles on aligned WO_3 nanotrees for super-hydrophilic thin films
Adv Mater, 21 (2009), pp. 1373-1376, 10.1002/adma.200802918

D. Zhang
Visible light-induced photocatalysis through surface plasmon excitation of platinum-metallized titania for photocatalytic bleaching of rhodamine B
Monatshefte Fur Chemie, 143 (2012), pp. 729-738, 10.1007/s00706-011-0631-2

Y.Z. Yang, C.H. Chang, H. Idriss
Photo-catalytic production of hydrogen form ethanol over M/TiO_2 catalysts (M = Pd, Pt or Rh)
Appl Catal B Environ, 67 (2006), pp. 217-222, 10.1016/j.apcatb.2006.05.007

K. Wenderich
Photodeposition of platinum nanoparticles on well-defined tungsten oxide (Doctoral Thesis)
University of Twente, Enschede (2016)

K.S.W. Sing, D.H. Everett, R.a.W. Haul, L. Moscou, R.a. Pierotti, J. Rouquérol, T. Siem ieniewska
INTERNATIONAL UNION OF pure commission ON colloid and surface chemistry including catalysis ∗ reporting physisorption data for GAS/SOLID systems with special reference to the determination of surface area and porosity
Pure Appl Chem, 54 (1982), pp. 2201-2218, 10.1351/pac198557040603

L. Ouyang, P.F. Tian, G.J. Da, X.C. Xu, C. Ao, T.Y. Chen, R. Si, J. Xu, Y.F. Han
The origin of active sites for direct synthesis of H_2O_2 on Pd/TiO_2 catalysts: interfaces of Pd and PdO domains
J Catal, 321 (2015), pp. 70-80, 10.1016/j.jcat.2014.10.003

J. Lee, W. Choi
Photocatalytic reactivity of surface platinized TiO_2: substrate specificity and the effect of Pt oxidation state
J Phys Chem B, 109 (2005), pp. 7399-7406, 10.1021/jp044425+

M. Bowker, C. Morton, J. Kennedy, H. Bahruji, J. Greves, W. Jones, P.R. Davies, C. Br ookes, P.P. Wells, N. Dimitratos
Hydrogen production by photoreforming of biofuels using Au, Pd and Au-Pd/TiO_2 photocatalysts
J Catal, 310 (2014), pp. 10-15, 10.1016/j.jcat.2013.04.005

J.A. Nasir, Z.U. Rehman, S.N.A. Shah, A. Khan, I.S. Butler, C.R.A. Catlow
Recent developments and perspectives in CdS-based photocatalysts for water splitting
J Mater Chem A, 8 (2020), pp. 20752-20780, 10.1039/d0ta05834c

J. Lian, D. Li, Y. Qi, N. Yang, R. Zhang, T. Xie, N. Guan, L. Li, F. Zhang
Metal-seed assistant photodeposition of platinum over Ta_3N_5 photocatalyst for promoted solar hydrogen production under visible light
J. Energy Chem., 55 (2021), 10.1016/j.jechem.2020.07.034

S. Bhardwaj, D. Dogra, B. Pal, S. Singh
Photodeposition time dependant growth, size and photoactivity of Ag and Cu deposited TiO_2 nanocatalyst under solar irradiation
Sol Energy, 194 (2019), 10.1016/j.solener.2019.10.055

R. Konta, T. Ishii, H. Kato, A. Kudo
Photocatalytic activities of noble metal ion doped $SrTiO_3$ under visible light irradiation
J Phys Chem, 108 (2004), pp. 8992-8995, 10.1021/jp049556p

J.F. Reber, K. Meier
Photochemical production of hydrogen with Zinc-sulfide suspensions
J Phys Chem, 88 (1984), pp. 5903-5913, 10.1021/j150668a032

Ratnawati Slamet, J. Gunlazuardi, E.L. Dewi
Enhanced photocatalytic activity of Pt deposited on titania nanotube arrays for the hydrogen production with glycerol as a sacrificial agent
Int J Hydrogen Energy, 42 (2017), pp. 24014-24025, 10.1016/j.ijhydene.2017.07.208

D.E. Santiago, J. Araña, O. González-Díaz, M.E. Alemán-Dominguez, A.C. Acosta-Dacal, C. Fernandez-Rodríguez, J. Pérez-Peña, J.M. Doña-Rodríguez
Effect of inorganic ions on the photocatalytic treatment of agro-industrial wastewaters containing imazalil
Appl Catal B Environ, 156–157 (2014), pp. 284-292, 10.1016/j.apcatb.2014.03.022

M. Jiménez-Tototzintle, I. Oller, A. Hernández-Ramírez, S. Malato, M.I. Maldonado
Remediation of agro-food industry effluents by biotreatment combined with supported TiO_2/H_2O_2 solar photocatalysis
Chem Eng J, 273 (2015), pp. 205-213, 10.1016/j.cej.2015.03.060

Z. Fan, S. Zhang, J. Liu, X. Hou
Effect of the chemical composition of formation water on gas well productivity
Chem Technol Fuels Oils, 50 (2014), pp. 252-256, 10.1007/s10553-014-0518-0

G.R. Bamwenda, S. Tsubota, T. Nakamura, M. Haruta
Photoassisted Hydrogen-Production from a water-ethanol solution - a Comparison of activities of Au-TiO_2 and Pt-TiO_2
J Photochem Photobiol Chem, 89 (1995), pp. 177-189, 10.1016/1010-6030(95)04039-I

K. Wenderich, K. Han, G. Mul

The effect of methanol on the photodeposition of Pt nanoparticles on tungsten oxide
Part Part Syst Char, 35 (2018), pp. 1-8, 10.1002/ppsc.201700250

R. Camposeco, S. Castillo, I. Mejía-Centeno, J. Navarrete, J. Marín
Characterization of physicochemical properties of Pd/TiO_2 nanostructured catalysts prepared by the photodeposition method
Mater Char, 95 (2014), pp. 201-210, 10.1016/j.matchar.2014.06.017

M.J. Weber
Atomic layer deposition of noble metal nanoparticles
(Doctoral Thesis)
Eindhoven University of Technology, Eindhoven (2014), 10.6100/IR776263

H. Kato, K. Asakura, A. Kudo
Highly efficient water splitting into H_2 and O_2 over lanthanum-doped $NaTaO_3$ photocatalysts with high crystallinity and surface nanostructure
J Am Chem Soc, 125 (2003), pp. 3082-3089, 10.1021/ja027751g

Y. Li, Y. Xie, S. Peng, G. Lu, S. Li
Photocatalytic hydrogen generation in the presence of chloroacetic acids over Pt/TiO_2
Chemosphere, 63 (2006), pp. 1312-1318, 10.1016/j.chemosphere.2005.09.004

R. Su, R. Tiruvalam, A.J. Logsdail, Q. He, C. A
Downing, M.T. Jensen, N. Dimitratos, L. Kesavan, P.P. Wells, R. Bechstein, *et al.*
Designer titania-supported Au-Pd nanoparticles for efficient photocatalytic hydrogen production
ACS Nano, 8 (2014), pp. 3490-3497, 10.1021/nn500963m

A. Patsoura, D.I. Kondarides, X.E. Verykios
Photocatalytic degradation of organic pollutants with simultaneous production of hydrogen
Catal Today, 124 (2007), pp. 94-102, 10.1016/j.cattod.2007.03.028

N. Strataki, V. Bekiari, D.I. Kondarides, P. Lianos
Hydrogen production by photocatalytic alcohol reforming employing highly efficient nanocrystalline titania films
Appl Catal B Environ, 77 (2007), pp. 184-189, 10.1016/j.apcatb.2007.07.015

W. Sun, S. Zhang, C. Wang, Z. Liu, Z. Mao
Effects of cocatalyst and calcination temperature on photocatalytic hydrogen evolution over $BaTi_4O_9$ powder synthesized by the polymerized complex method
Catal Lett, 123 (2008), pp. 282-288, 10.1007/s10562-008-9420-x

J. Rodríguez-Torres, C. Gómez-Solís, L.M. Torres-Martínez, I. Juárez-Ramírez
Synthesis and characterization of Au-Pd/$NaTaO_3$ multilayer films for photocatalytic hydrogen production
J Photochem Photobiol A Chem, 332 (2017), pp. 208-214, 10.1016/j.jphotochem.2016.08.026

Z.H.N. Al-zri, W.T. Chen, A. Chan, V. Jovic, T. Ina, H. Idriss, G.I.N. Waterhouse
The roles of metal co-catalysts and reaction media in photocatalytic hydrogen production: performance evaluation of M/TiO_2 photocatalysts (M = Pd, Pt, Au) in different alcohol-water mixtures
J Catal, 329 (2015), pp. 355-367, 10.1016/j.jcat.2015.06.005

W. Jones, D.J. Martin, A. Caravaca, A.M. Beale, M. Bowker, T. Maschmeyer, G. Hartle y, A. Masters
A comparison of photocatalytic reforming reactions of methanol and triethanolamine with Pd supported on titania and graphitic carbon nitride
Appl Catal B Environ (2017), pp. 1-7, 10.1016/j.apcatb.2017.01.042

H. Bahruji, M. Bowker, P.R. Davies, F. Pedrono
New insights into the mechanism of photocatalytic reforming on Pd/TiO_2
Appl Catal B Environ, 107 (2011), pp. 205-209, 10.1016/j.apcatb.2011.07.015

B.S. Kwak, J. Chae, J. Kim, M. Kang
Enhanced hydrogen production from methanol/water photo-splitting in TiO_2 including Pd component
Bull Kor Chem Soc, 30 (2009), pp. 253-2964

J. Romão, R. Salata, S.Y. Park, G. Mul
Photocatalytic methanol assisted production of hydrogen with simultaneous degradation of methyl orange
Appl Catal A Gen, 518 (2016), pp. 206-212, 10.1016/j.apcata.2015.10.020